Modelling Variability in Hot-Star Winds

Stanley P. Owocki[1]

Bartol Research Institute University of Delaware, Newark, DE 19716 USA

Abstract. I review 2-D hydrodynamical simulations of rotating hot-star winds with azimuthal structure induced by modulation of the radiative driving force near the wind base. As a first step toward examining more realistic perturbation mechanisms (e.g., nonradial pulsations, or magnetic fields), the driving modulation here is taken to arise from bright and dark spots in the stellar photophere. These spots induce decreases or increases in wind flow speed, and as the star rotates, spiral "Co-Rotating Interaction Regions" (CIRs) form, much as in the solar wind, from from interaction between fast and slow flow streams. A new feature unique to line-driven flow is a velocity-gradient kink that propagates inward from interaction fronts at a fast radiative-acoustic mode speed. The slowly evolving velocity plateaus that form behind such kinks give rise to absorption features with a slow apparent acceleration, much like the Discrete Absorption Components (DACs) often observed in UV wind lines from hot-stars. In simulation models with base driving sinusoidally modulated between increases and decreases, there arise alternating spiral streams of enhanced or decreased density, associated respectively with decreased or increase flow speeds. These speed variations have substantial impact on the line profile, and so these dynamical simulations are not as successful as analogous kinematic models of corotating density streams in reproducing the "phase-bowing" of periodic absorption modulations observed in the recent IUE 'Mega' project.

1 Introduction

Several papers at this meeting (e.g. by Prinja, Kaper, Kaufer, Massa, and Wolf) have summarized the extensive observational evidence for explicit variability, cyclical or otherwise, in the winds from hot, luminous, early type (OB) stars. A general challenge for theory is to understand the nature of the physical changes and/or structures associated with this variability. To be visible as direct variations in line-profiles formed from globally integrated radiative flux, the associated flow structure must be on a relatively large scale, on order the stellar radius. This makes it unlikely that such variations could stem from processes entirely *intrinsic* to the wind outflow, such as the inherent instability in the line-driving of the wind to small-scale perturbations (Rybicki 1987; Owocki, Castor, and Rybicki 1988; Owocki1994b). The dynamical evolution of such large-scale structure can be simulated using the local, computationally efficient, CAK/Sobolev expressions for the line force (Castor, Abbott, and Klein 1975; Sobolev 1960), making it feasible to carry out multidimensional simulations of the wind structure resulting from large-scale perturbations from the underlying, rotating star.

In this review, I will focus on recent efforts to develop initial dynamical models for two distinct classes of such variability, namely the 'classical' *Discrete*

Absorption Components (DACs) and the more recently identified *Periodic Absorption Modulations* (PAMs) discovered in the IUE 'Mega' project (Massa et al. 1995). Unlike the quasi-episodic, slowly evolving, net absorption enhancements that characterize most DACs, the PAMs recur regularly at periods a low order fraction of the rotation period, include both reductions and enhancements of absorption, and evolve relatively quickly over the line profile. Indeed, in contrast to the slow blueward evolution of DACs, the PAMs in one case (BO I star HD 64760) show a "phase-bowing" that reflects apparent redward as well as blueward propagation (Owocki, Cranmer, & Fullerton 1995; ; Fullerton et al. 1997). These distinct observational characteristics likely reflect differences in the underlying perturbation mechanisms, perhaps, for example, with the more stochastic DACs being induced by magnetic activity, and the regular PAMs being initiated by Non-Radial Pulsations (NRPs). But given the present uncertainty, the initial simulations here simply induce wind variations rather artificially, through direct modification of the radiative driving in the inner wind, much as might occur from "spots" on the underlying star (Cranmer and Owocki 1996, hereafter CO).

I first (§2) describe the effect of *isolated* spots, both brighter and darker than the ambiant photophere. As the star rotates, *Co-rotating Interaction Regions* (CIRs) form along spiral patterns by collision between faster and slower wind streams originating from different longitudes relative to the spot. These simulations thus represent the first dynamical test of the original proposal by Mullan (1984a,b; 1986) that the wind density enhancements in such CIRs could cause the DACs. A central goal here is to determine whether key characteristics of observed DACs, particularly their apparent slow acceleration, can be reproduced in synthetic line-profiles generated from dynamical models with CIRs.

I also examine (§3) the effect of a sinusoidal *modulation* of the radiative driving near the wind base, assuming a fixed number ($m = 4$) nodes around the star. This is intended as a dynamical version of the simple kinematic picture proposed to explain the "phase bowing" of the PAMs in HD 64760 (Owocki, Cranmer, & Fullerton 1995.) In this picture the PAMs arise from corotating streams of alternating increased or decreased density, within the key simplification that the velocity is fixed to a specific law, unaffected by the density perturbations. The dynamical simulations here self-consistently include such velocity variations, and so allow us to examine their effect in the line-formation.

2 CIRs Induced by Isolated Spots

Let us first review the CO simulations of wind structure induced by isolated spots on a rotating hot-star. The aim is to mimic physical processes – e.g. magnetic field, NRPs – that might increase or decrease the mass flux emerging from some localized region of the star, and then study how such variations are propagated through the radiatively driven stellar wind. To reduce the complexity and computational costs, the simulations are confined to 2-D variations in radius and azimuth (r, ϕ) within the equatorial plane. The line-driving force is computed using the standard CAK/Sobolev formalism (Castor, Abbott, Klein

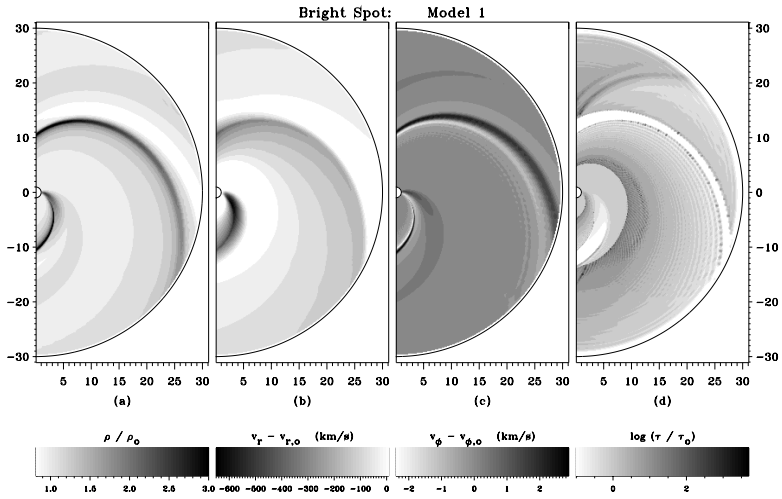

Fig. 1. Grayscale polar plots showing the spatial dependence of the deviations from a steady model for a. density, b. radial velocity, c. azimuthal velocity, and d. Sobolev optical depth.

1975; Sobolev 1960), modified by the finite-disk correction factor for a spherical outflow (Friend and Abbott 1986; Pauldrach, Puls, and Kudritzki 1986). This ignores the azimuthal force that should arise from sideview perspectives of the spot, and simply modifies the radial force by a fixed enhancement/reduction factor determined by the relative proximity to the spot.

The spot parameterization allows specification of both a longitudinal width Φ and an amplitude A, with $-1 < A < 0$ for dark spots and $A > 0$ for bright spots. Of the models listed in Table 1 of CO, I confine attention here to the first two, for which $\Phi = 20^o$ and $A = \pm 0.5$, representing a standard bright and dark spot. The stellar parameters represent those for the canonical O-type supergiant ζ Puppis, with a rotation speed $V_{rot} = 230$ km/s, corresponding to a rotation period of $P \approx 4.2$ days. For convenience, let us assume two identical spots positioned on opposite hemispheres, allowing restriction of the computation to an azimuth range of just 180^o with periodic boundary conditions.

For the bright spot case, figure 1 shows grayscale plots of the resulting density, radial velocity, azimuthal velocity, and radial Sobolev optical depth, all relative to values in the corresponding steady, spherically symmetric, CAK wind model without any spot. The spot here is centered on the x-axis, at the origin the spiral pattern of enhanced density that characterizes the resulting CIR. Note that regions of enhanced density generally correspond to regions of lower radial velocity. Because of the enhanced brightness over the spot, the wind driven from there initially has a higher mass flux, and thus higher density. As the enhanced brightness fades with increasing height above the spot, the higher density of this

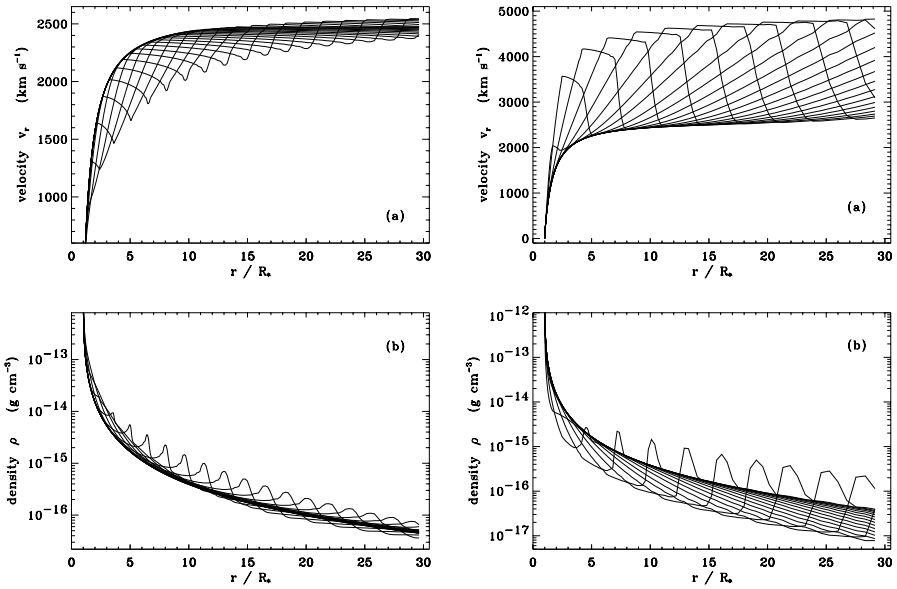

Fig. 2. left panels: Radial variation of velocity (upper panel) and density (lower panel) along selected, fixed azimuthal angles in the bright spot model.

Fig. 3. right panels: Same as fig. 2, but for the dark spot model.

material makes it harder to accelerate, reflecting the characteristic scaling of the line-acceleration with the inverse of the density ρ,

$$g_{lines} \sim \left[\frac{1}{\rho}\frac{\partial v_r}{\partial r}\right]^{\alpha} \qquad (1)$$

where α is the usual CAK exponent. The lower velocity gradient $\partial v_r/\partial r$ associated with the lower acceleration also contributes, through eq. (1), to a further reduction in the acceleration. As the stellar rotation brings this higher-density, lower-speed material into interaction with faster ambient wind originating away from the spot, there results a shock compression of the gas into the dense spiral stream that characterizes the CIR.

Though the general CIR formation here is analogous to that occuring in the solar wind (Hundhausen 1972; Zirker 1977), there are important differences. The much higher density of hot-star winds makes radiative cooling very efficient, and so the shocks are effectively isothermal. Unlike the nearly adiabatic shocks in the solar wind, which have a maximum compression ratio of four in the strong shock limit, the density compression in such isothermal shocks scales with the square of the Mach number, and so can be arbitarily large. Moreover, whereas the nearly adiabatic shocks of the solar wind propagate backward into the faster wind at roughly a quarter of the shock speed, these isothermal shocks remain in close proximity to the compressed layer.

Another significant difference arises when we consider the nature of the *pre-shock* flow. In ordinary gas-dynamics (or even MHD) shocks, the preshock flow is assumed to be completely unaffected by the impending shock, simply because the speed of this material exceeds the sound speed (or in MHD, the fast-mode speed), preventing any upwind information propagation that a disturbance lies ahead. However, as first shown by Abbott (1980), the characteristic speeds $c_\pm$ in a *line-driven* flow are substantially modified by the operation of the line force, given by

$$c_\pm \;=\; -U/2 \pm \sqrt{(U/2)^2 + a^2}, \tag{2}$$

where a is the ordinary (isothermal) sound speed, and $U \equiv \partial g_{lines}/\partial(\partial v_r/\partial r)$ is a new characteristic speed, nowadays often called the "Abbott speed". From eqn. (1) we find $U \sim g_{lines}/(\partial v_r/\partial r)$, but from the radial equation of motion, we expect $v_r \partial v_r/\partial r \sim g_r$, which suggests $U \sim v_r$, i.e. this Abbott wave speed is typically of order the radial flow speed. Since most the wind is supersonic, we find $v_r \approx U \gg a$, implying that *inward* wave propagation can now occur at a speed $c_- \approx -U \approx -v_r$ that is much *faster* than the propagation of an ordinary sound wave (Owocki and Rybicki 1985, 1986; Rybicki, Owocki, & Castor 1990).

Figure 2 shows line plots of the radial variation of (a) velocity and (b) density along selected, fixed azimuthal angles. The location of the compressed CIR is apparent from the velocity minima and density maxima. But note that the velocity has a *decreasing* outward gradient over a broad region ahead of this CIR, extending back to a velocity gradient discontinuity, or "kink", that marks the connection to the unperturbed, outward-accelerating wind. This weak, kink discontinuity propagates inward (relative to the wind outflow) at roughly the characteristic speed $c_- \approx -U$, and since this is nearly as fast as the local outflow speed, it has only a slow net outward propagation in the fixed stellar frame.

Such fast inward-propagation of a velocity-gradient kink is a novel and quite unique feature of a line-driven flow, and it has potentially important consequences for interpreting observed line-profile features, particularly DACs. To identify which wind structures should yield the most prominent profile variations, let us examine the radial Sobolev optical depth,

$$\tau_r(r,\phi) \;=\; \frac{\kappa v_{th} \rho(r,\phi)}{|\partial v_r/\partial r|}. \tag{3}$$

The line absorption coefficient κ and the ion thermal speed v_{th} are assumed to have the same, constant value in the perturbed and unperturbed wind. Thus the variations in optical depth ratio plotted in figure 1d reflect changes in the ratio of density over velocity-gradient. Surprisingly, we see from comparison with figure 1a that the regions of strongest optical depth enhancements do not occur within the dense CIR compression, but rather within the shallow velocity-gradient region immediately after the kink.

The emergent flux line-profiles from this wind structure can be readily synthesized using the standard SEI (Sobolev source function with Exact Integration) method of Lamers et al. (1987), generalized for 3-D integration as described in CO. For this purpose, the 3-D latitudinal structure is derived by interpolation

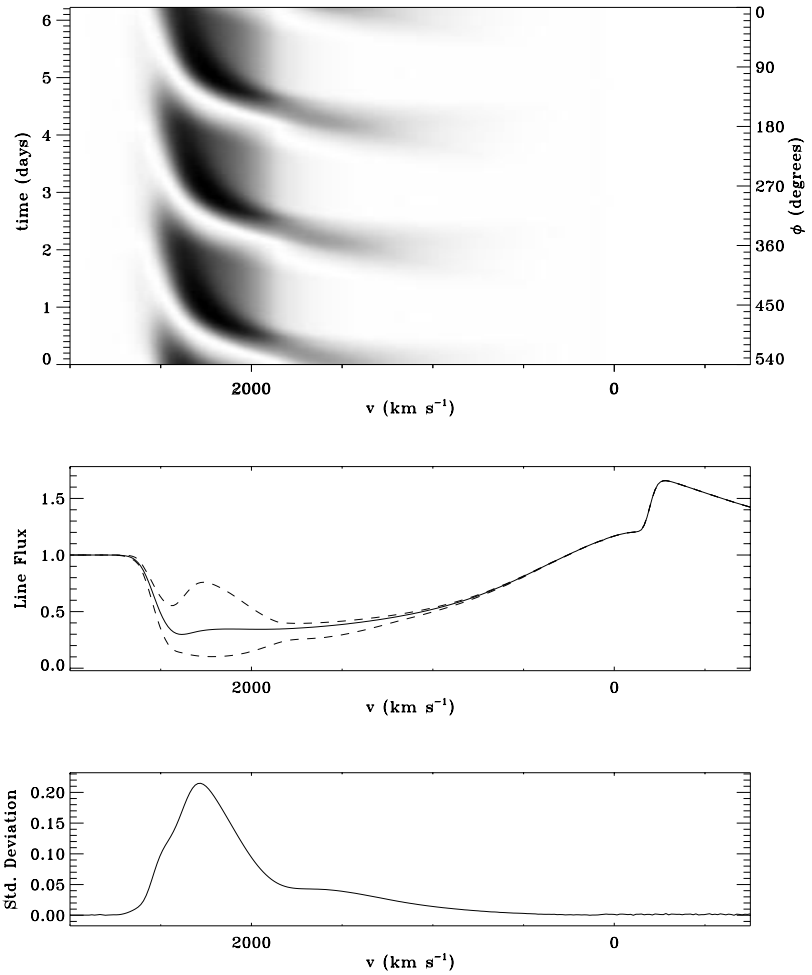

Fig. 4. Line profile variation for marginally thick line as a function velocity and time. In the middle box, the solid line shows the unperturbed wind profile, and the dashed lines show the extrema for each velocity. The bottom box shows the profile standard deviation.

from the equator to a polar model characterized by a 1-D, unperturbed wind solution. For a moderate strength line that is marginally optically thick in the wind, figure 4 shows a grayscale plot of the profile variation as a function of frequency (in velocity units) and time. The latter is derived from simple mapping of the azimuthal coordinate ϕ using the star's rotation frequency Ω, i.e. $t = (\phi - \phi_o)/\Omega$, where ϕ_o is defined such that the observer is directly over the spot at the initial time $t = 0$. Following observational convention, the gray scale here is scaled to the range from mininum to maximum flux at each frequency, with the maxi-

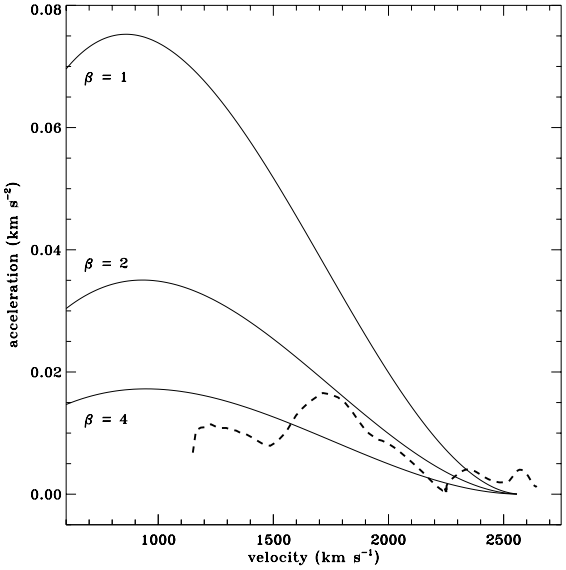

Fig. 5. Apparent acceleraton vs. velocity for bright-spot model DAC, compared to velocity laws with various exponents β.

mum flux (i.e., minimum absorption) corresponding to the lightest shade. This convention is suitable for describing the observed DACs that represent mainly enhanced absorption relative to the background wind. But the synthetic profile variations here also show intervals of *reduced* absorption, reflecting the relative reduction of the density in the region just beyond the CIR.

As noted above, the absorption enhancements here arise primarily from regions of shallow velocity-gradient near the reverse mode kinks. Because of the slow net outward propagation of these kinks, the associated synthetic DACs migrate quite *slowly* blueward across the profile over roughly ~ 3.9 day, in general agreement with the slow apparent acceleration of observed DACs. Often this slow accleration is characterized in terms of large values of the exponent β in the canonical velocity law given by $v(r) = v_\infty(1 - R_*/r)^\beta$. Figure 5 plots the apparent acceleration vs. velocity for the synthetic DAC compared with results for velocity laws with various β. Whereas an unperturbed wind is expected to have a velocity law with $\beta \approx 1$, fig. 4 shows that the DAC in this model corresponds more closely to higher exponents $\beta \approx 2 - 4$, much as inferred for observed DACs.

Let us next briefly consider results for the case of a "dark" spot, wherein the radiative driving is reduced at base of the wind outflow. In this case, the mass flux emerging from the spot region is now reduced, and as the radiative driving recovers at greater heights above the spot, the reduced density causes an enhanced acceleration, which then results in a very fast stream. Figure 3 shows the radial variation of velocity and density at selected fixed angles. Note the velocities ranging up to 5000 km/s, more than double the maximum speed in

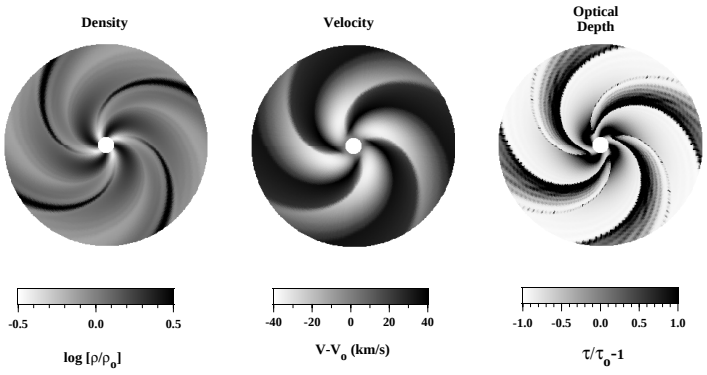

Fig. 6. Spatial variation of density, velocity and Sobolev optical depth, normalized relative to the unperturbed model, for the case with $m = 4$ sinusoidal modulation in azimuth.

the unperturbed wind, and much higher than is ever observed in line-profiles of such an O-supergiant. This implies that such reduced mass flux regions cannot be very prominent in hot-star winds. In particular, it argues against the importance of hot-star analogs of solar coronal holes (Zirker 1977), with very high-speed wind streams arising from regions of rapidly diverging open magnetic field (cf. MacGregor 1988).

3 Co-rotating Streams from Sinusoidal Modulations

An important result of the IUE 'Mega' campaign was the identification of the clearly cyclical PAMs in wind line profiles of several stars. In the case of the B0 I star HD 64760, these PAMs show a "phase-bowing" that suggests apparent redward as well as blueward propagation. Owocki, Cranmer, and Fullerton (1996) have shown that such bowing can be reproduced from a simple kinematic model with co-rotating spiral streams of alternating regions of increased and reduced density. This kinematic model ignores any dynamical effect these density variations might have in inducing corresponding velocity changes. As an initial attempt to extend this kinematic picture into a dynamically self-consistent model, let us next briefly consider the response of a line-driven wind to a perturbation that varies *sinusoidally* in azimuth between enhanced and reduced radiative driving.

Figure 6 shows grescale plots of the changes in density, velocity, and Sobolev optical depth for such a dynamical model with an azimuthal period of 90^o and

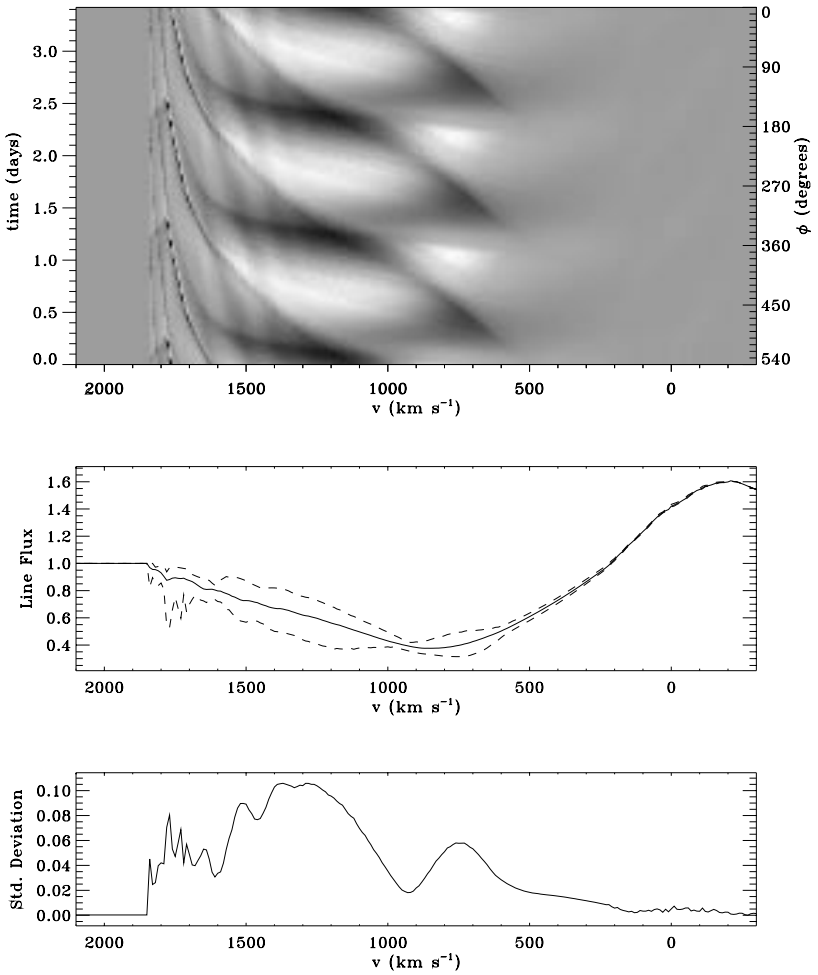

Fig. 7. As in fig. 4, but for the sinusoidally modulated model.

perturbations amplitdue of $A = 0.5$. Note that there are substantial effects on the velocity as well as density, and that the optical depth variations no longer just follow the density, as was assumed in the heuristic corotating stream model for the observed phase-bowing. Figure 7 shows the quite complex profile variability for the line profile of a moderatel strong in this sinusoidal modulation model. The complexity reflects the intricate interdependence of flow variations in density, velocity, and velocity gradient. The comparitively simple phase-bowing pattern of the kinematic model is not apparent here. Indeed, it is not clear what sort of dynamically consistent structure could give the observed phase-bowing.

4 Concluding Remarks

The simulations here demonstrate that the physical dependencies of line-driving play an important role in the dynamical evolution of wind structure, and lead to phenomena, e.g., the reverse-mode kink, that have no analog in ordinary gas dynamics. The inward propagation of this kink yield the slow net outward propagation of a velocity plateau flow pattern that causes the enhanced absorption, providing one possible explanation for the relatively slow apparent acceleration in observed DACs. However, such models typically also predict line-profile features that not commonly seen, most notably *reduced* absorption components. Thus, an alternative mechanism for producing slow DACs is a substantial increase, i.e. factor of two or more, in the mass being ejected into the wind, without a compensating increase in the driving. The acceleration of such material can be especially slow, and so the extra absorption from its higher density could also form slowly evolving DACs (Owocki, Fullerton, and Puls 1994).

As for the PAMs observed in the IUE mega project, we find that dynamical models with periodic modulation typically show substantial velocity variations that complicate the line-profile signature. In particular, the simple, phenomenalogical, kinematic picture developed to explain phase bowing cannot be easily adapted to a fully self-consistent dynamical model.

The work described here represents only the first steps in trying to develop dynamically self-consistent models of the flow structure assoicated with the observed variability of hot-star winds. In the future, models should address more directly the two most obvious possible perturbation mechanisms, namely nonradial pulsations and surface magnetic fields, with particular emphasis on identifying observatonal characteristic that could help in distinguishing which mechanism is most responsible for each of various kinds of observed wind variability. Within such studies, it will remain helpful to contrast the inferred flow structures with those derived for the sun and other cool stars, and in particular to identify which characteristics are peculiar to the dynamics of radiative driving by line-scattering. The cyclical variability of hot-stars thus provides an unique potential for studying this important aspect of radiation hydrodynamics.

Acknowledgements: This work was supported in part by NASA grant NAGW-2624. Supporting computations were carried out using an allocation of supercomputer time from the San Diego Supercomputer Center. Much of the research reviewed here was carried out in collaboration with S. Cranmer, as part of his Ph. D. thesis. I also acknowledge numerous helpful discussions with A. Fullerton, K. Gayley, H. Henrichs, L. Kaper, and J. Puls.

References

Abbott, D. C. 1980, Ap. J., 242, 1183
Castor, J. I., Abbott, D. C., & Klein, R. I. 1975, Ap. J., 195, 157 (CAK)
Cranmer, S. R., & Owocki, S. P. 1996, Ap. J., 469, 469
Friend, D. B., & Abbott, D. C. 1986, Ap. J., 311, 701
Fullerton, A. W., & Owocki, S. P. 1992, in
Fullerton, A. W., Massa, D. L., Prinja, R. K., Owocki, S. P., and Cranmer, S. R. 1997, Astron. & Ap., 327, 699
Hundhausen, A. J. 1972, Coronal Expansion and Solar Wind (Berlin: Springer-Verlag)
Lamers, H. J. G. L. M., Cerruti-Sola, M., & Perinotto, M. 1987, Ap. J., 314, 726
MacGregor, K. B. 1988, Ap. J., 327, 794
Massa, D., et al. 1995, Ap. J.l, 452, L53
Mullan, D. J. 1984a, Ap. J., 283, 303
Mullan, D. J. 1984b, Ap. J., 284, 769
Mullan, D. J. 1986, Astron. & Ap., 165, 157
Owocki, S. P. 1994, in IAU Symp. 162, Pulsation, Rotation, and Mass Loss in Early-Type Stars, ed. L. A. Balona, H. F. Henrichs, & J. M. Le Contel (Dordrecht: Kluwer), 475
Owocki, S. P. 1994, Ap. Sp. Sci., 221, 1
Owocki, S. P., Castor, J. I., & Rybicki, G. B. 1988, Ap. J., 335, 914
Owocki, S. P., Cranmer, S. R., & Fullerton, A. W. 1995, Ap. J.l, 453, L37
Owocki, S. P., Fullerton, A. W., & Puls, J. 1994, Ap. Sp. Sci., 221, 437
Owocki, S. P., & Rybicki, G. B. 1985, Ap. J., 199, 365
Owocki, S. P., & Rybicki, G. B. 1986, Ap. J., 209, 127
Pauldrach, A. W. A., Puls, J., & Kudritzki, R.-P. 1986, Astron. & Ap., 164, 86
Pizzo, V. J. 1982, J. Geophys. Res., 87, 4374
Rybicki, G. B. 1987, in Instabilities in Luminous Early Type Stars, ed. H. J. G. L. M. Lamers & C. W. H. de Loore (Dordrecht: Reidel), 175
Rybicki, G. B., Owocki, S. P., & Castor, J. I. 1990, Ap. J., 349, 274
Sobolev, V. V. 1960, Moving Envelopes of Stars (Cambridge: Harvard University Press)
Zirker, J. B., ed. 1977, Coronal Holes and High Speed Wind Streams (Boulder: Colorado Associated University Press)

Henrichs: We, as observers, would like to thank you very much for the so many years of fundamental calculations you did, that helped enormously to interpret the data on stellar wind variability. You showed even an example that is far ahead of any observations I have seen so far. For obvious reasons you put your perturbing spot on the stellar equator, but in practice such a spot is most likely at higher latitude. Would that not change the predicted behavior drastically? Could you comment?

Owocki: Perturbations away from the equator obviously require a 3-D simulation, which with modern computers is readily doable, though not yet attempted. In the context of CIRs in the solar wind, V. Pizzo in the 1970's already developed 3-D models, showing some interesting new effects not possible in 2-D, e.g. flow around the CIR at other latitudes. In rapidly rotating hot stars, an additional effect may be deflection toward or away from the equator. This remains a problem to be investigated.